Received 18 March 2020; | Revised ; | Accepted

DOI: xxx/xxxx

RESEARCH ARTICLE

Analytical solutions describing the oblique flow of a viscous incompressible fluid around a dendritic crystal

Dmitri V. Alexandrov[1*] | Peter K. Galenko[2]

[1]Department of Theoretical and Mathematical Physics, Laboratory of Multi-Scale Mathematical Modeling, Ural Federal University, Ekaterinburg, Russian Federation
[2]Physikalisch-Astronomische Fakultät, Friedrich-Schiller-Universität Jena, Jena, Germany

Correspondence
*Dmitri V. Alexandrov, Department of Theoretical and Mathematical Physics, Laboratory of Multi-Scale Mathematical Modeling, Ural Federal University, Ekaterinburg, Russian Federation. Email: dmitri.alexandrov@urfu.ru

This article considers the hydrodynamic problem of an oblique flow of a viscous incompressible fluid around the tip of a dendritic crystal. Approximate analytical solutions of Oseen's hydrodynamic equations are obtained in 2D and 3D cases using special curvilinear coordinates. It is shown that the projections of the fluid velocity change significantly with a change in the flow slope and Reynolds number. The theory developed in this work has a limiting transition to the previously known solutions for the rectilinear (without tilt) fluid flow around a dendrite.

KEYWORDS:
hydrodynamics, dendrites, applied mathematical modeling, crystal growth

1 | INTRODUCTION

It is well known that the dendritic shape of crystals is one of the most common growth forms in the processes of phase transformations from metastable solutions and melts.[1−10] As this takes place, the shape of the dendrite vertex is described by a power function close to a parabola (paraboloid) at distances of the order of several radii of curvature of its tip.[11] Quite often, in nature, technological processes, and laboratory experiments, dendrites grow in the oncoming convective flow of a viscous liquid (melt or solution).[12−15] In addition, such a liquid flow can be directed at an angle to the direction of crystal growth or change its direction during crystallization. This fluid flow, as is known, leads to a redistribution of temperature and impurities dissolved in the fluid (the fluid flow rate is involved in the equations of convective heat conduction and diffusion of impurities, as well as in the boundary conditions to them). Therefore, it becomes necessary to solve the hydrodynamic problem of an oblique flow of a viscous fluid around a dendrite growing in a metastable fluid. The solution of such a hydrodynamic problem is also in demand in the theory of selecting a stable mode of dendritic growth in inclined flows of an undercooled (supersaturated) liquid.[16−18]

Taking into account the above-described practical relevance, in this article, a solution to the hydrodynamic problem of an oblique flow of a viscous fluid around a two-dimensional (three-dimensional) dendritic crystal is derived. Since the Navier-Stokes equations for this flow geometry do not have exact solutions, we use here the Oseen hydrodynamic equations.[19−21] Strictly speaking, the Oseen system of equations takes place at low Reynolds numbers. However, in some cases, these equations describe fluid flows at Reynolds numbers of the order of unity.[21]

This paper is organized as follows. The governing equations for an oblique flow occurring around two- and three-dimensional dendritic crystals are formulated and analytically solved in Section 2. Here the solution is also rewritten in the reference frame connected with a growing dendrite. A behaviour of hydrodynamic solutions under consideration as well as the main outcomes and future developments of the theory are given in Section 3.

2 | GOVERNING EQUATIONS

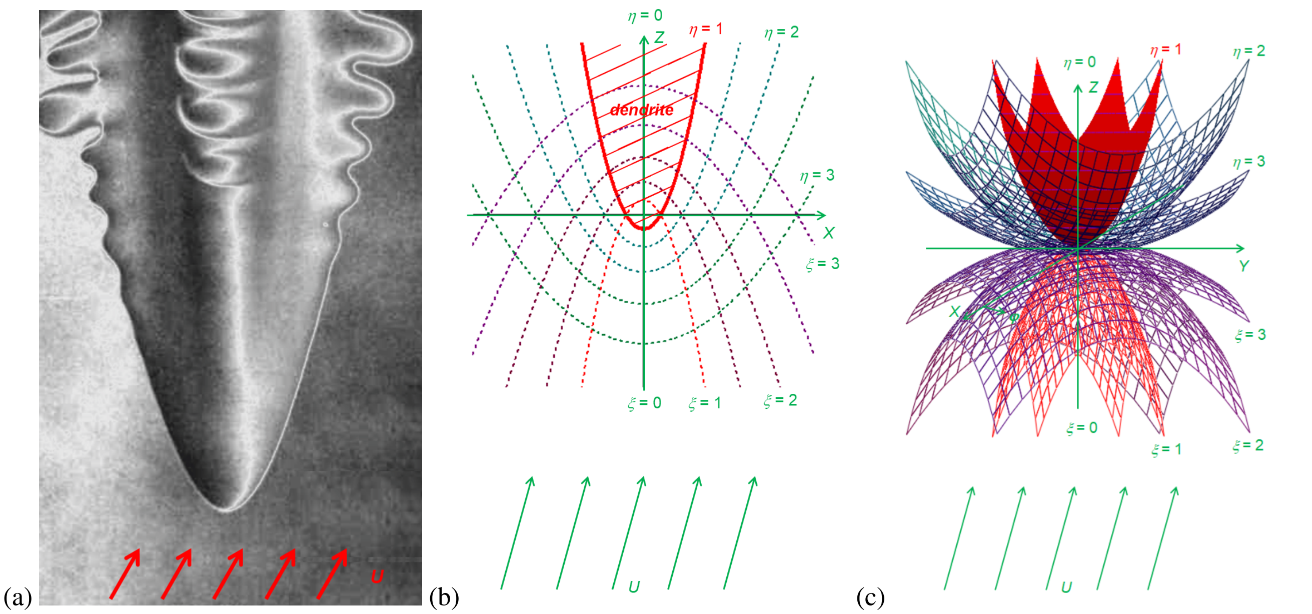

FIGURE 1 A tip region of dendritic crystal in an oblique flow of a viscous fluid (a) and the coordinate systems of a parabolic cylinder (b) and a paraboloid of revolution (c) describing its growth.

2.1 | Parabolic/paraboloidal reference frames

Suppose the vertex of a dendritic crystal is parabolic/paraboloidal. This makes it possible to use the following curvilinear coordinates when describing two- and three-dimensional fluid flows around dendrites (see figure 1).

The parabolic cylinder reference frame ξ and η (two-dimensional dendrite) is related to the Cartesian reference frame x, y and z as follows

$$\frac{z}{\rho} = Z = \frac{\xi^2 - \eta^2}{2}, \ \frac{y}{\rho} = Y = Y, \ \frac{x}{\rho} = X = \xi\eta, \tag{1}$$

where ρ - stands for the dendrite tip diameter. Note that the crystal surface in parabolic coordinates (1) takes the form $\eta = 1$. As this takes place, the fluid is in the domain $0 \le \xi < \infty$ and $1 < \eta < \infty$.

The unit vectors in both coordinate sytems read as

$$\mathbf{e}_z = \frac{\xi \mathbf{e}_\xi - \eta \mathbf{e}_\eta}{\sqrt{\xi^2 + \eta^2}}, \ \mathbf{e}_x = \frac{\eta \mathbf{e}_\xi + \xi \mathbf{e}_\eta}{\sqrt{\xi^2 + \eta^2}}. \tag{2}$$

To find the partial derivatives in hydrodynamic equations, we use the Lamé coefficients

$$h_\xi = h_\eta = \rho\sqrt{\xi^2 + \eta^2}, \ h_y = \rho. \tag{3}$$

Using (2) and (3) one can get the following expressions

$$\frac{\partial}{\partial Z} = \frac{\xi}{\xi^2 + \eta^2}\frac{\partial}{\partial \xi} - \frac{\eta}{\xi^2 + \eta^2}\frac{\partial}{\partial \eta}, \ \frac{\partial}{\partial X} = \frac{\eta}{\xi^2 + \eta^2}\frac{\partial}{\partial \xi} + \frac{\xi}{\xi^2 + \eta^2}\frac{\partial}{\partial \eta}. \tag{4}$$

The paraboloid of revolution reference frame ξ, η and φ (three-dimensional dendrite) is related to the Cartesian reference frame x, y and z as follows

$$\frac{z}{\rho} = Z = \frac{\xi^2 - \eta^2}{2}, \ \frac{y}{\rho} = Y = \xi\eta \sin\varphi, \ \frac{x}{\rho} = X = \xi\eta\cos\varphi. \tag{5}$$

As before, the crystal surface is given by $\eta = 1$, and the fluid is in the domain $0 \le \xi < \infty$, $1 < \eta < \infty$ and $0 \le \varphi < 2\pi$.

The unit vectors and Lamé coefficients have the form

$$\mathbf{e}_z = \frac{\xi \mathbf{e}_\xi - \eta \mathbf{e}_\eta}{\sqrt{\xi^2+\eta^2}},\ \mathbf{e}_y = \frac{\eta \sin\varphi \mathbf{e}_\xi + \xi \sin\varphi \mathbf{e}_\eta}{\sqrt{\xi^2+\eta^2}} - \cos\varphi \mathbf{e}_\varphi,\ \mathbf{e}_x = \frac{\eta \cos\varphi \mathbf{e}_\xi + \xi \cos\varphi \mathbf{e}_\eta}{\sqrt{\xi^2+\eta^2}} + \sin\varphi \mathbf{e}_\varphi, \tag{6}$$

$$h_\xi = h_\eta = \rho\sqrt{\xi^2+\eta^2},\ h_\varphi = \rho\xi\eta. \tag{7}$$

Taking (6) and (7) into account, we arrive at

$$\frac{\partial}{\partial Z} = \frac{\xi}{\xi^2+\eta^2}\frac{\partial}{\partial \xi} - \frac{\eta}{\xi^2+\eta^2}\frac{\partial}{\partial \eta},\ \frac{\partial}{\partial Y} = \frac{\eta\sin\varphi}{\xi^2+\eta^2}\frac{\partial}{\partial \xi} + \frac{\xi\sin\varphi}{\xi^2+\eta^2}\frac{\partial}{\partial \eta} - \frac{\cos\varphi}{\xi\eta}\frac{\partial}{\partial\varphi}, \tag{8}$$

$$\frac{\partial}{\partial X} = \frac{\eta\cos\varphi}{\xi^2+\eta^2}\frac{\partial}{\partial \xi} + \frac{\xi\cos\varphi}{\xi^2+\eta^2}\frac{\partial}{\partial \eta} + \frac{\sin\varphi}{\xi\eta}\frac{\partial}{\partial\varphi}. \tag{9}$$

2.2 | The Oseen hydrodynamic equations

We describe the flow of a viscous incompressible fluid around a dendritic crystal using linear Oseen equations. Methods for solving these equations are well-known in modern literature.[19–22] We use here the approach developed by Dash and Gill.[21] So, the hydrodynamic model takes the form of

$$\mathbf{U}\cdot\nabla\mathbf{u} = -\frac{1}{\rho_l}\nabla p + \nu\nabla^2\mathbf{u},\ \nabla\cdot\mathbf{u} = 0. \tag{10}$$

Here $\mathbf{u} = (u, v, w)$ is the fluid velocity with components u, v, w on the coordinate axes z, y, x, $\mathbf{U} = (U_z, U_y, U_x)$ stands for the fluid velocity far from the solid surface $\eta = 1$ with coordinates U_z, U_y, U_x, ρ_l - is the density, p is the pressure, ν is the kinematic viscosity.

These equations should be supplemented with the following boundary conditions

$$u = v = w = 0,\ \eta = 1;\ u \to U_z,\ v \to U_y,\ w \to U_x,\ \eta \to \infty. \tag{11}$$

For the convenience of solving the problem, we use the relative velocities

$$u' = u - U_z,\ v' = v - U_y,\ w' = w - U_x, \tag{12}$$

$n = U_y/U_z$, $l = U_x/U_z$ and the Reynolds number $\text{Re} = U_z\rho/\nu$. Taking these designations into account, we rewrite (10) as

$$\text{Re}\frac{\partial u'}{\partial Z} + n\text{Re}\frac{\partial u'}{\partial Y} + l\text{Re}\frac{\partial u'}{\partial X} = -\frac{\rho}{\rho_l \nu}\frac{\partial p}{\partial Z} + \frac{\partial^2 u'}{\partial Z^2} + \frac{\partial^2 u'}{\partial Y^2} + \frac{\partial^2 u'}{\partial X^2}, \tag{13}$$

$$\text{Re}\frac{\partial v'}{\partial Z} + n\text{Re}\frac{\partial v'}{\partial Y} + l\text{Re}\frac{\partial v'}{\partial X} = -\frac{\rho}{\rho_l \nu}\frac{\partial p}{\partial Y} + \frac{\partial^2 v'}{\partial Z^2} + \frac{\partial^2 v'}{\partial Y^2} + \frac{\partial^2 v'}{\partial X^2}, \tag{14}$$

$$\text{Re}\frac{\partial w'}{\partial Z} + n\text{Re}\frac{\partial w'}{\partial Y} + l\text{Re}\frac{\partial w'}{\partial X} = -\frac{\rho}{\rho_l \nu}\frac{\partial p}{\partial X} + \frac{\partial^2 w'}{\partial Z^2} + \frac{\partial^2 w'}{\partial Y^2} + \frac{\partial^2 w'}{\partial X^2}, \tag{15}$$

$$\frac{\partial u'}{\partial Z} + \frac{\partial v'}{\partial Y} + \frac{\partial w'}{\partial X} = 0. \tag{16}$$

In addition, expressions (11) read as

$$u' = -U_z,\ v' = -U_y,\ w' = -U_x,\ \eta = 1;\ u' \to 0,\ v' \to 0,\ w' \to 0,\ \eta \to \infty. \tag{17}$$

2.3 | Complete solutions of 2D and 3D models

For the convenience of finding analytical solutions, we introduce additional functions M and N

$$u' = \frac{\partial M}{\partial Z} + \frac{1}{\text{Re}}\frac{\partial N}{\partial Z} - N,\ v' = \frac{\partial M}{\partial Y} + \frac{1}{\text{Re}}\frac{\partial N}{\partial Y} - nN, \tag{18}$$

$$w' = \frac{\partial M}{\partial X} + \frac{1}{\text{Re}}\frac{\partial N}{\partial X} - lN,\ p = -\frac{\rho_l \nu}{\rho}\text{Re}\left(\frac{\partial M}{\partial Z} + n\frac{\partial M}{\partial Y} + l\frac{\partial M}{\partial X}\right). \tag{19}$$

In the two-dimensional case, $v' = 0$ and M is independent on Y.

Substitution of (18) and (19) into (13)-(16) leads to

$$\frac{\partial^2 M}{\partial Z^2}+\frac{\partial^2 M}{\partial Y^2}+\frac{\partial^2 M}{\partial X^2}=0,\ \frac{\partial^2 N}{\partial Z^2}+\frac{\partial^2 N}{\partial Y^2}+\frac{\partial^2 N}{\partial X^2}-\mathrm{Re}\left(\frac{\partial N}{\partial Z}+n\frac{\partial N}{\partial Y}+l\frac{\partial N}{\partial X}\right)=0. \tag{20}$$

An important point is that we consider the problem in the vicinity of the dendritic tip where ξ is small. Keeping this in mind, assuming $M=M(\eta)$ and $N=N(\eta)$, we rewrite (20) with the help of (4), (8), (9), and arrive at

$$\text{2D case}:\ \frac{d^2 M}{d\eta^2}=0,\ \frac{d^2 N}{d\eta^2}+\mathrm{Re}\eta\frac{dN}{d\eta}=0, \tag{21}$$

$$\text{3D case}:\ \frac{d^2 M}{d\eta^2}+\frac{1}{\eta}\frac{dM}{d\eta}=0,\ \frac{1}{\eta}\frac{d}{d\eta}\left(\eta\frac{dN}{d\eta}\right)+\mathrm{Re}\eta\frac{dN}{d\eta}=0. \tag{22}$$

The solution of equations (21) and (22) has the form

$$\text{2D case}:\ M(\eta)=A_1\eta+B_1,\ N(\eta)=C_1\int_1^{\eta}\exp\left(-\frac{\mathrm{Re}t^2}{2}\right)dt+C_2, \tag{23}$$

$$\text{3D case}:\ M(\eta)=A_2\ln\eta+B_2,\ N(\eta)=D_1\int_1^{\eta}\exp\left(-\frac{\mathrm{Re}t^2}{2}\right)\frac{dt}{t}+D_2. \tag{24}$$

Substitution of (23) and (24) into (17), (18) and (19) enables us to find the arbitrary constants

$$A_1=A_2=-\frac{C_1\exp(-\mathrm{Re}/2)}{\mathrm{Re}},\ C_1^{-1}=-C_2^{-1}\int_1^{\infty}\exp\left(-\frac{\mathrm{Re}t^2}{2}\right)dt, \tag{25}$$

$$D_1^{-1}=-D_2^{-1}\int_1^{\infty}\exp\left(-\frac{\mathrm{Re}t^2}{2}\right)\frac{dt}{t},\ C_2=D_2=U_z. \tag{26}$$

Let us especially highlight that expressions (18) and (19) do not include B_1 and B_2 since the components u', v' and w' are the functions of $M(\eta)$-derivatives only. Taking (12), (18), (19), (25), and (26) into account, we come to

$$u=U_z\left\{1-\frac{\mathrm{erfc}\left(\sqrt{\mathrm{Re}/2}\eta\right)}{\mathrm{erfc}\left(\sqrt{\mathrm{Re}/2}\right)}-\frac{\eta\left[\exp\left(-\mathrm{Re}/2\right)-\exp\left(-\mathrm{Re}\eta^2/2\right)\right]}{\sqrt{\pi\mathrm{Re}/2}\left(\xi^2+\eta^2\right)\mathrm{erfc}\left(\sqrt{\mathrm{Re}/2}\right)}\right\}, \tag{27}$$

$$w=U_z\left\{l\left[1-\frac{\mathrm{erfc}\left(\sqrt{\mathrm{Re}/2}\eta\right)}{\mathrm{erfc}\left(\sqrt{\mathrm{Re}/2}\right)}\right]+\frac{\xi\left[\exp\left(-\mathrm{Re}/2\right)-\exp\left(-\mathrm{Re}\eta^2/2\right)\right]}{\sqrt{\pi\mathrm{Re}/2}\left(\xi^2+\eta^2\right)\mathrm{erfc}\left(\sqrt{\mathrm{Re}/2}\right)}\right\} \tag{28}$$

in 2D geometry and

$$u=U_z\left\{1-\frac{\mathrm{E}_1\left(\mathrm{Re}\eta^2/2\right)}{\mathrm{E}_1\left(\mathrm{Re}/2\right)}-\frac{2\left[\exp\left(-\mathrm{Re}/2\right)-\exp\left(-\mathrm{Re}\eta^2/2\right)\right]}{\mathrm{Re}\left(\xi^2+\eta^2\right)\mathrm{E}_1\left(\mathrm{Re}/2\right)}\right\}, \tag{29}$$

$$v=U_z\left\{n\left[1-\frac{\mathrm{E}_1\left(\mathrm{Re}\eta^2/2\right)}{\mathrm{E}_1\left(\mathrm{Re}/2\right)}\right]+\frac{2\xi\sin\varphi\left[\exp\left(-\mathrm{Re}/2\right)-\exp\left(-\mathrm{Re}\eta^2/2\right)\right]}{\mathrm{Re}\left(\xi^2+\eta^2\right)\eta\mathrm{E}_1\left(\mathrm{Re}/2\right)}\right\}, \tag{30}$$

$$w=U_z\left\{l\left[1-\frac{\mathrm{E}_1\left(\mathrm{Re}\eta^2/2\right)}{\mathrm{E}_1\left(\mathrm{Re}/2\right)}\right]+\frac{2\xi\cos\varphi\left[\exp\left(-\mathrm{Re}/2\right)-\exp\left(-\mathrm{Re}\eta^2/2\right)\right]}{\mathrm{Re}\left(\xi^2+\eta^2\right)\eta\mathrm{E}_1\left(\mathrm{Re}/2\right)}\right\} \tag{31}$$

in 3D geometry. Note that

$$\mathrm{erfc}(q)=\frac{2}{\sqrt{\pi}}\int_q^{\infty}\exp\left(-\kappa^2\right)d\kappa,\ \mathrm{E}_1(q)=\int_q^{\infty}\frac{\exp\left(-\kappa\right)}{\kappa}d\kappa.$$

An important point is that this solution contains the previously studied case of symmetric flow: $n=l=0$. Indeed, (27)-(31) lead to formulas (68) and (69)[21] if $n=l=0$.

Representing the velocity vector in component-wise form $\mathbf{u} = u\mathbf{e}_z + v\mathbf{e}_y + w\mathbf{e}_x = u_\xi \mathbf{e}_\xi + u_\eta \mathbf{e}_\eta + u_\varphi \mathbf{e}_\varphi$ and taking (2) and (6) into consideration, we arrive at

$$u_\xi = \frac{U_z(\xi + l\eta)}{\sqrt{\xi^2+\eta^2}}\left(1 - \frac{\mathrm{erfc}\left(\sqrt{\mathrm{Re}/2}\eta\right)}{\mathrm{erfc}\left(\sqrt{\mathrm{Re}/2}\right)}\right), \tag{32}$$

$$u_\eta = \frac{U_z}{\sqrt{\xi^2+\eta^2}}\left\{(l\xi - \eta)\left[1 - \frac{\mathrm{erfc}\left(\sqrt{\mathrm{Re}/2}\eta\right)}{\mathrm{erfc}\left(\sqrt{\mathrm{Re}/2}\right)}\right] + \frac{\exp(-\mathrm{Re}/2) - \exp\left(-\mathrm{Re}\eta^2/2\right)}{\sqrt{\pi \mathrm{Re}/2}\,\mathrm{erfc}\left(\sqrt{\mathrm{Re}/2}\right)}\right\} \tag{33}$$

in 2D geometry and

$$u_\xi = \frac{U_z(\xi + n\eta\sin\varphi + l\eta\cos\varphi)}{\sqrt{\xi^2+\eta^2}}\left(1 - \frac{\mathrm{E}_1\left(\mathrm{Re}\eta^2/2\right)}{\mathrm{E}_1(\mathrm{Re}/2)}\right), \tag{34}$$

$$\begin{aligned} u_\eta = \frac{U_z}{\sqrt{\xi^2+\eta^2}}\Bigg[&(n\xi\sin\varphi + l\xi\cos\varphi - \eta)\left(1 - \frac{\mathrm{E}_1\left(\mathrm{Re}\eta^2/2\right)}{\mathrm{E}_1(\mathrm{Re}/2)}\right) \\ &+ \frac{2\left[\exp(-\mathrm{Re}/2) - \exp\left(-\mathrm{Re}\eta^2/2\right)\right]}{\mathrm{Re}\,\eta \mathrm{E}_1(\mathrm{Re}/2)}\Bigg], \end{aligned} \tag{35}$$

$$u_\varphi = U_z(l\sin\varphi - n\cos\varphi)\left(1 - \frac{\mathrm{E}_1\left(\mathrm{Re}\eta^2/2\right)}{\mathrm{E}_1(\mathrm{Re}/2)}\right) \tag{36}$$

in 3D geometry. Let us again note that (32)-(36) are identical to (70)-(75)[21] if $l = n = 0$.

2.4 | Hydrodynamic solutions in the reference frame of a moving crystal

For the convenience of mathematical modeling of crystal growth, a frame of reference is often used that moves with the dendrite. Let the origin of such a coordinate system coincides with the radius of curvature of the crystal tip. Also, we use below the modified coordinates accordingly to many previous studies[16,23–28]

$$\text{2D}: \; z = \frac{\rho}{2}(\eta - \xi), \; x = \rho\sqrt{\xi\eta}; \; \text{3D}: \; z = \frac{\rho}{2}(\eta - \xi), \; y = \rho\sqrt{\xi\eta}\sin\varphi, \; x = \rho\sqrt{\xi\eta}\cos\varphi. \tag{37}$$

Let us introduce the opposite coordinate axis z of the dendrite evolving with an unchangeable rate V. In this case, one can get

$$u_\xi = \frac{V\sqrt{\xi}}{\sqrt{\xi+\eta}} + \frac{U_z\left(\sqrt{\xi} + l\sqrt{\eta}\right)}{\sqrt{\xi+\eta}}\left(1 - \frac{\mathrm{erfc}\left(\sqrt{\mathrm{Re}\eta/2}\right)}{\mathrm{erfc}\left(\sqrt{\mathrm{Re}/2}\right)}\right), \tag{38}$$

$$u_\eta = -\frac{V\sqrt{\eta}}{\sqrt{\xi+\eta}} + \frac{U_z}{\sqrt{\xi+\eta}}\left\{\left(l\sqrt{\xi} - \sqrt{\eta}\right)\left[1 - \frac{\mathrm{erfc}\left(\sqrt{\mathrm{Re}\eta/2}\right)}{\mathrm{erfc}\left(\sqrt{\mathrm{Re}/2}\right)}\right] + \frac{\exp(-\mathrm{Re}/2) - \exp(-\mathrm{Re}\eta/2)}{\sqrt{\pi\mathrm{Re}/2}\,\mathrm{erfc}\left(\sqrt{\mathrm{Re}/2}\right)}\right\} \tag{39}$$

in the 2D case, and

$$u_\xi = \frac{V\sqrt{\xi}}{\sqrt{\xi+\eta}} + \frac{U_z\left(\sqrt{\xi} + n\sqrt{\eta}\sin\varphi + l\sqrt{\eta}\cos\varphi\right)}{\sqrt{\xi+\eta}}\left(1 - \frac{\mathrm{E}_1(\mathrm{Re}\eta/2)}{\mathrm{E}_1(\mathrm{Re}/2)}\right), \tag{40}$$

$$\begin{aligned} u_\eta = -\frac{V\sqrt{\eta}}{\sqrt{\xi+\eta}} + \frac{U_z}{\sqrt{\xi+\eta}}\Bigg[&\left(n\sqrt{\xi}\sin\varphi + l\sqrt{\xi}\cos\varphi - \sqrt{\eta}\right)\left(1 - \frac{\mathrm{E}_1(\mathrm{Re}\eta/2)}{\mathrm{E}_1(\mathrm{Re}/2)}\right) \\ &+ \frac{2\left[\exp(-\mathrm{Re}/2) - \exp(-\mathrm{Re}\eta/2)\right]}{\mathrm{Re}\sqrt{\eta}\mathrm{E}_1(\mathrm{Re}/2)}\Bigg], \end{aligned} \tag{41}$$

$$u_\varphi = U_z(l\sin\varphi - n\cos\varphi)\left(1 - \frac{\mathrm{E}_1(\mathrm{Re}\eta/2)}{\mathrm{E}_1(\mathrm{Re}/2)}\right) \tag{42}$$

in the 3D case. It is significant that expressions (38)-(42) transform to the corresponding solutions in the case of a direct (with zero angle) liquid flow to the dendrite ($l = n = 0$).[16,29]

3 | DISCUSSION AND CONCLUSION

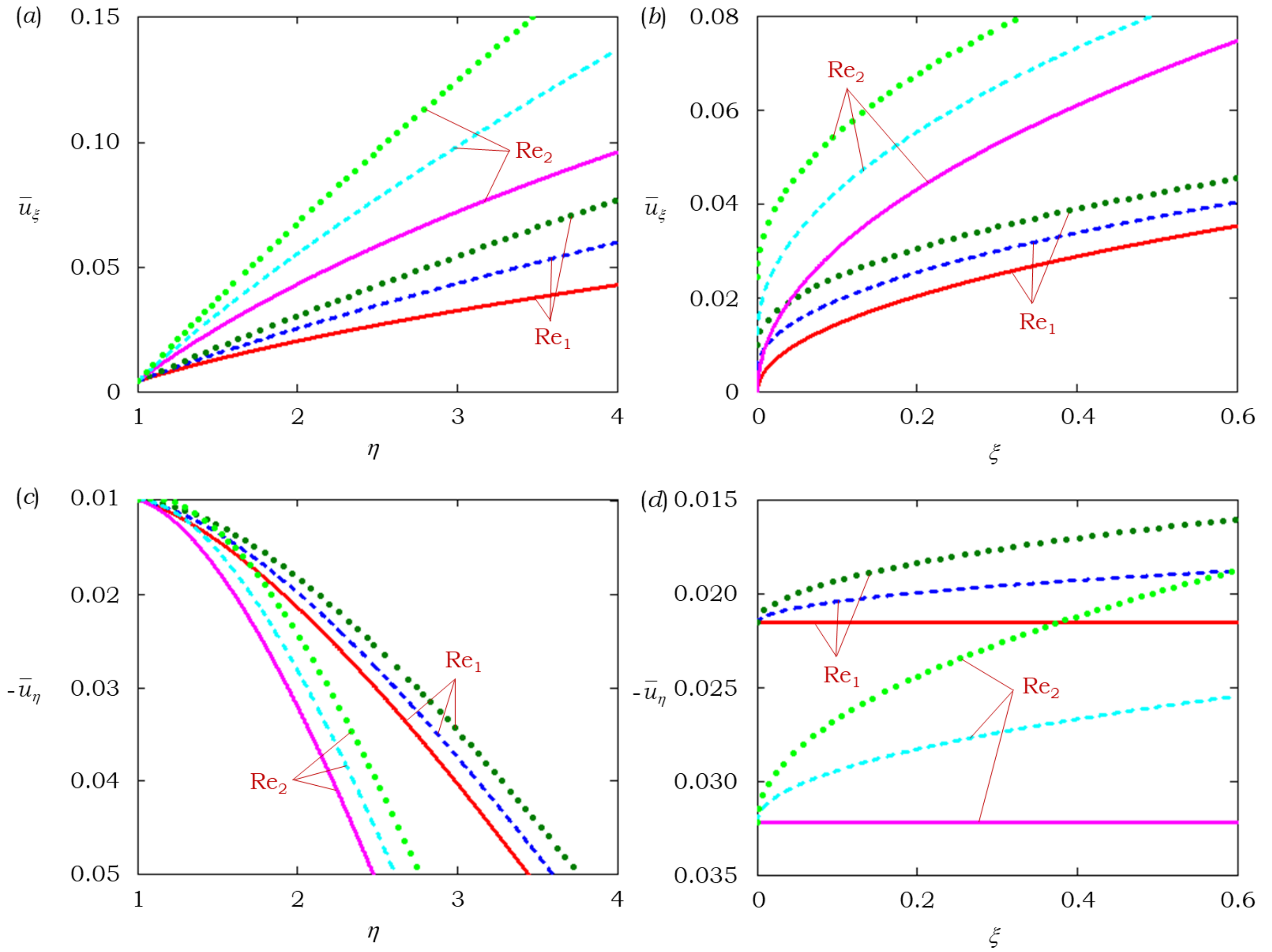

FIGURE 2 2D solutions. The modified velocities $\bar{u}_\xi = u_\xi\sqrt{\xi+\eta}/U_z$ (panels a, b) and $\bar{u}_\eta = u_\eta\sqrt{\xi+\eta}/U_z$ (panels c, d) versus the spatial variables η ($\xi = 0.2$) and ξ ($\eta = 2$) accordingly to solutions (38) and (39) in cases of $l = 0$ (solid curves), $l = 0.1$ (dashed curves), and $l = 0.2$ (dotted curves); $\mathrm{Re}_1 = 0.01$, $\mathrm{Re}_2 = 0.05$, and $V/U_z = 0.01$.

Figures 2 and 3 illustrate the role of hydrodynamic flow slope $l = U_x/U_z$ and Reynolds number $\mathrm{Re} = U_z\rho/\nu$ on modified velocity projections $\bar{u}_\xi = u_\xi\sqrt{\xi+\eta}/U_z$ and $\bar{u}_\eta = u_\eta\sqrt{\xi+\eta}/U_z$ in accordance with analytical solutions (38)-(41). Our calculations demonstrate that both velocity projections change quite strongly with a slight change in the hydrodynamic slope. As this takes place, small variations in Reynolds number also have a significant effect on the distribution of the components of the hydrodynamic flow. Such significant changes in the distribution of the flow velocity must lead to a change in the temperature and concentration fields around the dendrite tip. This is caused by the corresponding changes in the convective terms in the equations of heat conduction and diffusion of impurities.

Another important circumstance is the asymmetry of the inclined flow relative to the dendrite axis. This, obviously, should lead to a change in the direction of its growth when the angle of inclination of the hydrodynamic flow changes. And this, in turn, entails a change in the main parameters of stable growth of the dendritic vertex - its diameter and velocity. Therefore, one of the directions of research development is to determine the criterion for stable dendritic growth in oblique hydrodynamic flows in the spirit of the previously constructed theory[4,15,16,29] for flows with a zero inclination coefficient to the axis of dendritic growth. In

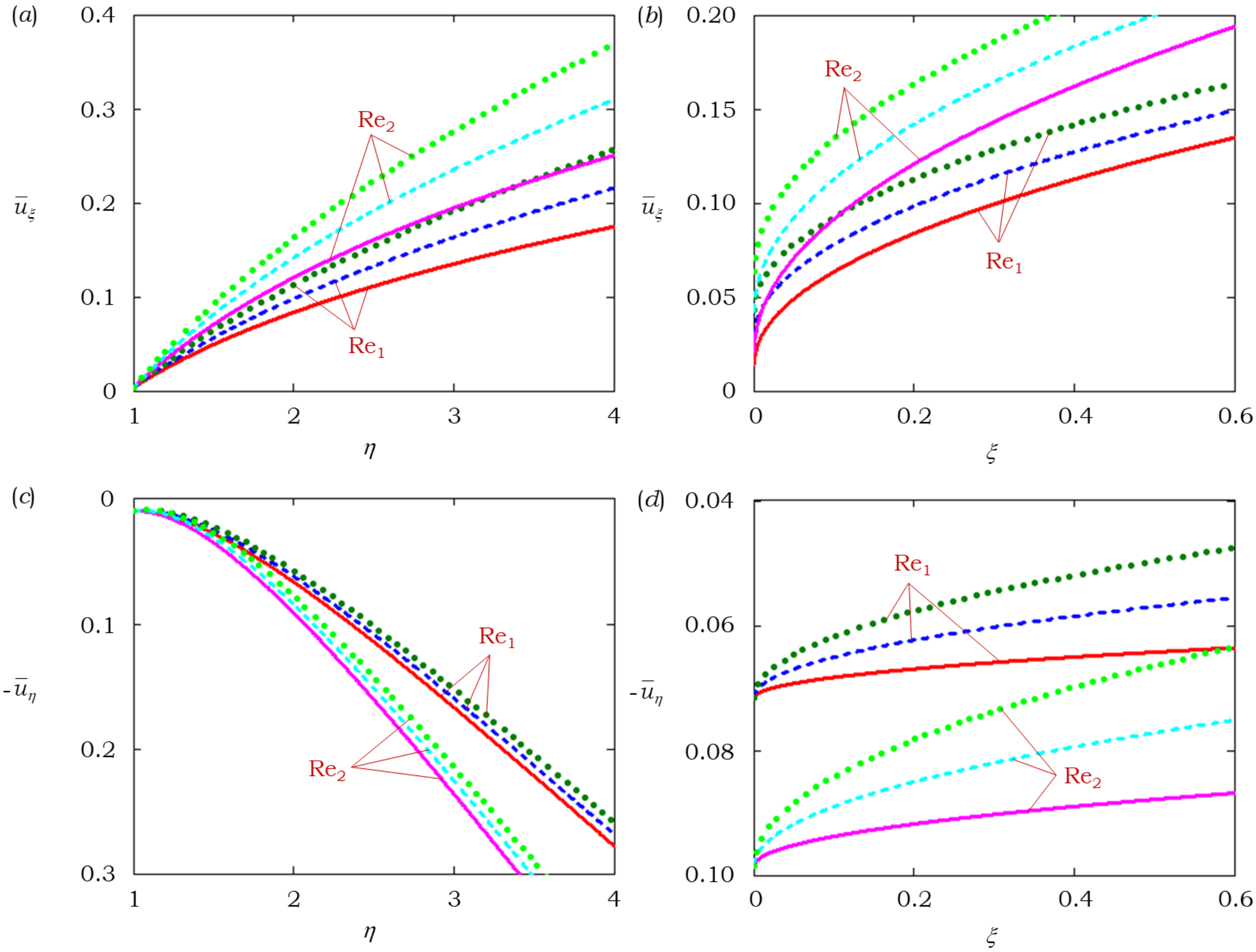

FIGURE 3 3D solutions. The modified velocities $\bar{u}_\xi = u_\xi\sqrt{\xi+\eta}/U_z$ (panels a, b) and $\bar{u}_\eta = u_\eta\sqrt{\xi+\eta}/U_z$ (panels c, d) versus the spatial variables η ($\xi = 0.2$) and ξ ($\eta = 2$) accordingly to solutions (40) and (41) in cases of $l = 0$ (solid curves), $l = 0.1$ (dashed curves), and $l = 0.2$ (dotted curves); $\mathrm{Re}_1 = 0.01$, $\mathrm{Re}_2 = 0.05$, $V/U_z = 0.01$, $n = 0.1$, and $\varphi = \pi/4$.

addition, oblique flows of supercooled melts and supersaturated solutions should lead to a more complex structure of secondary branches of dendritic crystals in the phase transformation region. In general, growth forms in such a two-phase region in the presence of inclined flows should differ significantly from the forming microstructure in the absence of a flow or the presence of a rectilinear (non-oblique) fluid flow. The development of the theory of phase transformation in such a two-phase zone is also an important direction of scientific research, which can be carried out by analogy with several existing theories.[30–45]

ACKNOWLEDGMENTS

This work contains two parts, theoretical and numerical. The first of them was supported by the Russian Foundation for Basic Research (project no. 19-32-51009). The second part was supported by the Ministry of Science and Higher Education of the Russian Federation [project no. FEUZ-2020-0057].

Author contributions

The authors contributed equally to the present research article.

Conflict of interest

The authors declare no potential conflict of interests.

ORCID

Dmitri V. Alexandrov https://orcid.org/0000-0002-6628-745X
Peter K. Galenko https://orcid.org/0000-0003-2941-7742

References

1. Huang S-C, Glicksman ME. Overview 12: Fundamentals of dendritic solidification – II development of sidebranch structure. *Acta Metall.* 1981;29:717–734.

2. Galenko PK, Alexandrov DV. From atomistic interfaces to dendritic patterns. *Phil Trans R Soc A.* 2018;376:20170210.

3. Shibkov AA, Zheltov MA, Korolev AA, Kazakov AA, Leonov AA. Crossover from diffusion-limited to kinetics-limited growth of ice crystals. *J Cryst Growth.* 2005;285:215–227.

4. Alexandrov DV, Galenko PK, Toropova LV. Thermo-solutal and kinetic modes of stable dendritic growth with different symmetries of crystalline anisotropy in the presence of convection. *Phil Trans R Soc A.* 2018;376:20170215.

5. Alexandrov DV, Galenko PK. Selected mode for rapidly growing needle-like dendrite controlled by heat and mass transport. *Acta Mater.* 2017;137:64–70.

6. Yokoyama E, Yoshizaki I, Shimaoka T, Sone T, Kiyota T, Furukawa Y. Measurements of growth rates of an ice crystal from supercooled heavy water under microgravity conditions: basal face growth rate and tip velocity of a dendrite. *J Phys Chem B.* 2011;115:8739–8745.

7. Yokoyama E, Yoshizaki I, Shimaoka T, Sone T, Kiyota T, Furukawa Y. Precise measurements of dendrite growth of ice crystals in microgravity. *Microgravity Sci Technol.* 2012;24:245–253.

8. Huang W, Wang L. Solidification researches using transparent model materials – A review. *Sci China Technol Sci.* 2012;55:377–386.

9. Alexandrov DV, Galenko PK, Herlach DM. Selection criterion for the growing dendritic tip in a non-isothermal binary system under forced convective flow. *J Cryst Growth.* 2010;312:2122-2127.

10. Galenko PK, Danilov DA, Reuther K, Alexandrov DV, Rettenmayr M, Herlach DM. Effect of convective flow on stable dendritic growth in rapid solidification of a binary alloy. *J Cryst Growth.* 2017;457:349–355.

11. Alexandrov DV, Galenko PK. The shape of dendritic tips. *Phil Trans R Soc A.* 2020;378:20190243.

12. Herlach D, Galenko P, Holland-Moritz D. *Metastable Solids from Undercooled Melts*. Amsterdam: Elsevier; 2007.

13. Bouissou P, Perrin B, Tabeling P. Influence of an external flow on dendritic crystal growth. *Phys Rev A.* 1989;40:509–519.

14. Gao J, Kao A, Bojarevics V, Pericleous K, Galenko PK, Alexandrov DV. Modeling of convection, temperature distribution and dendritic growth in glass-fluxed nickel melts. *J Cryst Growth.* 2017;471:66–72.

15. Alexandrov DV, Galenko PK. Selection criterion of stable mode of dendritic growth with n-fold symmetry at arbitrary Péclet numbers with a forced convection. In: Gutschmidt S, Hewett JN, Sellier M, eds. *IUTAM Symposium on Recent Advances in Moving Boundary Problems in Mechanics*, IUTAM Bookseries 34. Springer 2019 (pp. 203–215).

16. Bouissou P, Pelcé P. Effect of a forced flow on dendritic growth. *Phys Rev A.* 1989;40:6673–6680.

17. Alexandrov DV, Galenko PK. Dendritic growth with the six-fold symmetry: theoretical predictions and experimental verification. *J Phys Chem Solids.* 2017;108:98–103.

18. Alexandrov DV, Galenko PK. Selected mode of dendritic growth with n-fold symmetry in the presence of a forced flow. *EPL.* 2017;119:16001.

19. Lamb H (Sir). *Hydrodynamics*. Cambridge: Cambridge University Press; 1895.

20. Kochin NE, Kibel' IA, Roze NV. *Theoretical Hydromechanics*. New York: Interscience; 1964.

21. Dash SK, Gill WN. Forced convection heat and momentum transfer to dendritic structures (parabolic cylinders and paraboloids of revolution). *Int J Heat Mass Trans.* 1984;27:1345–1356.

22. Buyevich YuA, Alexandrov DV, Zakharov SV. *Hydrodynamics: Examples and Problems*. New York, Wallingford, UK: Begell House, Inc.; 2001.

23. Alexandrov DV, Galenko PK. Thermo-solutal and kinetic regimes of an anisotropic dendrite growing under forced convective flow. *Phys Chem Chem Phys.* 2015;17:19149–19161.

24. Alexandrov DV, Danilov DA, Galenko PK. Selection criterion of a stable dendrite growth in rapid solidification. *Int J Heat Mass Trans.* 2016;101:789–799.

25. Pelcé P. *Dynamics of Curved Fronts*. Boston, MA: Academic Press; 1988.

26. Ben Amar M, Pelcé P. Impurity effect on dendritic growth. *Phys Rev A.* 1989;39:4263–4269.

27. Galenko PK, Alexandrov DV, Titova EA. The boundary integral theory for slow and rapid curved solid/liquid interfaces propagating into binary systems. *Phil Trans R Soc A.* 2018;376:20170218.

28. Alexandrov DV, Galenko PK. Thermo-solutal growth of an anisotropic dendrite with six-fold symmetry. *J Phys Condens Matter.* 2018;30:105702.

29. Alexandrov DV, Galenko PK. Dendrite growth under forced convection: Analysis methods and experimental tests. *Phys-Usp.* 2014;57:771–786.

30. Hills RN, Loper DE, Roberts PH. A thermodynamically consistent model of a mushy zone. *Q J Appl Maths.* 1983;36:505–539.

31. Fowler AC. The formation of freckles in binary alloys. *IMA J Appl Math.* 1985;35:159–174.

32. Borisov VT. *Theory of Two-Phase Zone of a Metal Ingot*. Moscow: Metallurgiya Publishing House; 1987.

33. Alexandrov DV, Malygin AP. Coupled convective and morphological instability of the inner core boundary of the Earth. *Phys Earth Planet Inter.* 2011;189:134–141.

34. Alexandrova IV, Alexandrov DV, Aseev DL, Bulitcheva SV. Mushy layer formation during solidification of binary alloys from a cooled wall: the role of boundary conditions. *Acta Phys Polonica A.* 2009;115:791–794.

35. Alexandrov DV, Bashkirtseva IA, Ryashko LB. Nonlinear dynamics of mushy layers induced by external stochastic fluctuations. *Phil Trans R Soc A.* 2018;376:20170216.

36. Alexandrova IV, Alexandrov DV. Dynamics of particulate assemblages in metastable liquids: a test of theory with nucleation and growth kinetics. *Phil Trans R Soc A.* 2020;378:20190245.

37. Aseev DL, Alexandrov DV. Unidirectional solidification with a mushy layer. The influence of weak convection. *Acta Mater..* 2006;54:2401–2406.

38. Makoveeva EV, Alexandrov DV. Effects of nonlinear growth rates of spherical crystals and their withdrawal rate from a crystallizer on the particle-size distribution function. *Phil Trans R Soc A.* 2019;377:20180210.

39. Ivanov AA, Alexandrova IV, Alexandrov DV. Phase transformations in metastable liquids combined with polymerization. *Phil Trans R Soc A.* 2019;377:20180215.

40. Nizovtseva IG, Alexandrov DV. The effect of density changes on crystallization with a mushy layer. *Phil Trans R Soc A.* 2020;378:20190248.

41. Alexandrov DV, Ivanov AA. Solidification of a ternary melt from a cooled boundary, or nonlinear dynamics of mushy layers. *Int J Heat Mass Trans.* 2009;52:4807–4811.

42. Alexandrov DV, Nizovtseva IG, Malygin AP, Huang H-N, Lee D. Unidirectional solidification of binary melts from a cooled boundary: Analytical solutions of a nonlinear diffusion-limited problem. *J Phys Condens Matter.* 2008;20:114105.

43. Alexandrov DV, Ivanov AA, Alexandrova IV. Analytical solutions of mushy layer equations describing directional solidification in the presence of nucleation. *Phil Trans R Soc A.* 2018;376:20170217.

44. Alexandrov DV, Malygin AP. Flow-induced morphological instability and solidification with the slurry and mushy layers in the presence of convection. *Int J Heat Mass Trans.* 2012;55:3196–3204.

45. Alexandrov DV. On the theory of Ostwald ripening in the presence of different mass transfer mechanisms. *J. Phys Chem Solids.* 2016;91:48–54.

How to cite this article: Alexandrov D.V., and Galenko P.K. (2021), Analytical solutions describing the oblique flow of a viscous incompressible fluid around a dendritic crystal, *Math Meth Appl Sci.*,